

# 1 On the use of satellite-derived frontal metrics in time series analyses 2 of shelf-sea fronts, a study of the Celtic Sea

---

3 Lavinia A. Suberg<sup>a,\*,#</sup>, Peter I. Miller<sup>b</sup>, Russell B. Wynn<sup>a</sup>

4  
5 <sup>a</sup> National Oceanography Centre- Southampton, European Way, Southampton, S014 3ZH,  
6 UK

7 <sup>b</sup> Remote Sensing Group, Plymouth Marine Laboratory, Prospect Place, Plymouth PL1 3DH,  
8 UK

9  
10 <sup>#</sup> Current Address: Centre Ifremer Bretagne, ZI Pointe du Diable, CS 10070, 29280 Plouzane,  
11 France

12  
13 \*Corresponding author

14 Email address: [lsuberg@ifremer.fr](mailto:lsuberg@ifremer.fr) (L.Suberg)

15  
16  
17 **Keywords:** Frontal metrics, Shelf-sea fronts, Time series analysis, Satellite imagery, Celtic  
18 Sea

## 19 20 **Author contributions:**

21 LS and RW developed the concept. Monthly level-4 composites of the various frontal metrics  
22 used in the analysis were provided by PM as 8bit raster files. Data processing and analysis  
23 was carried out by LS. Manuscript was written by LS and revised by all authors.

## 24 25 26 **Abstract**

27 Satellite-derived frontal metrics describe characteristics of oceanic thermal fronts, such as  
28 their strength or persistence. They are used in marine science to investigate spatio-temporal  
29 variability of thermal fronts or in ecological studies to assist in explaining animal  
30 distributions. Although the metrics are based on sometimes complex algorithms, little  
31 guidance is available on their correct application in quantitative analyses, in particular for  
32 non-specialist users. This research aims to improve accurate use of frontal data. This case  
33 study investigates the inter-annual and seasonal variability of two tidal mixing fronts on the  
34 Celtic Sea shelf, based on monthly time series of daily frontal maps at  $\sim 1\text{km}^2$  resolution from  
35 1990 to 2010. Some metrics are almost identical and can be grouped, e.g. *frontal probability*,  
36 *persistence* and so-called “*composites*” (Pearson correlation:  $r=0.8-1.0$ ;  $p<0.001$ ), whereas a  
37 metric describing frontal *strength* was distinct from other ones. *Strength* and metrics of the  
38 *frontal probability* group showed pronounced differences in their inter-annual and seasonal  
39 variability: *Strength* displayed an oscillating pattern between 1990 and 2010 while there were  
40 no significant changes in *probability* over time. In addition, seasonal variability estimates  
41 were affected by frontal segments not belonging to the fronts of interest, which could result  
42 in biased estimates. Most important, there was a doubling of available satellite imagery

43 between 1990 and 2010 due to a greater number of operational satellites, which negatively  
44 affected frontal *probability*, *positively frontal strength* and consequently, changed the  
45 temporal pattern of both. When using frontal maps for temporal analyses, we should choose  
46 the metric carefully, be aware of biased estimates caused by variability from unwanted frontal  
47 segments in the data and account for the variable data availability. This clear guide on the use  
48 of frontal metrics will be helpful to improve correct interpretations of statistical analyses.  
49

## 50 **1 Introduction**

51 Marine thermal fronts are transition zones in which steep gradients in temperature can be  
52 observed over a relatively small distance, often associated with changes in other physical  
53 properties, complex hydrodynamics and elevated biomass. Thermal fronts occur over a wide  
54 range of spatio-temporal scales, ranging from the large-scale Polar Front to small, short-lived  
55 tidal intrusion (Owen, 1981). Frontal metrics derived from remote sensing satellite imagery  
56 describe characteristics of these thermal fronts, such as their strength or frequency, in the area  
57 of interest and for a desired period. They come in the form of images called frontal maps,  
58 which are usually a fusion of multiple satellite images, because single images are often cloud-  
59 covered (Miller, 2009). Combining multiple images into one map creates (ideally) a cloud  
60 free view on the ocean surface. The resulting frontal maps are a mosaic of pixels containing  
61 values describing a front (frontal values) or not (cloud free pixel that cover an area of sea  
62 without fronts). The frontal maps provide information on the surface signal of thermal fronts  
63 over large spatio-temporal scales, which makes them very popular for scientists from a  
64 variety of backgrounds, including oceanographers and ecologists.  
65

66 Frontal maps are particularly applicable to the study of large-scale processes because of their  
67 spatio-temporal coverage: a global and contiguous time series since the 1980's. They have  
68 been used to describe their spatio-temporal variability (Hopkins et al. 2010; Lee et al., 2015;  
69 Park et al. 2007; Belkin et al., 2009; Nieblas et al. 2014; Oram et al. 2008) and to create maps  
70 of surface fronts all over the world (e.g. Canary Upwelling System: Nieto et al., 2012; the  
71 Pacific Ocean: Belkin and Cornillon, 2003; Canadian waters: Cry & Larouche, 2015;  
72 California Current System: Armstrong et al., 2012; Indian Ocean: Roa-Pascuali et al. 2015).  
73 Satellite-derived frontal metrics have also become popular in recent years amongst marine  
74 ecologists to explain and predict species distributions, particularly for marine apex predators  
75 (e.g. Bauer et al. 2015; Nieto et al. 2017; Priede et al. 2009;). The potential of fronts to act as  
76 biodiversity hotspots has also received attention from policymakers involved in development  
77 of spatial conservation measures such as Marine Protected Areas (MPAs), and future

78 monitoring of mobile species as part of the Marine Strategy Framework Directive (MSFD)  
79 (Defra, 2009;2012; European Union, 2008). Initially, frontal maps were used only  
80 descriptively and compared to tracks or distribution maps of marine biota (Doniol-Valcroze et  
81 al., 2007; Edwards et al., 2013; McClathie et al. 2012; Wingfield et al. 2011). Now, they are  
82 increasingly being used in statistical models to investigate bio-physical coupling and  
83 ecosystem dynamics (Broodie et al. 2015; Pirotta et al., 2014; Xu et al. 2017).

84

85

86 Frontal metrics represent highly processed data and can be based on complex algorithms,  
87 making it difficult for the user to understand the meaning and their limitations when applying  
88 statistical analyses, particular for scientist not specialist in the field of remote frontal  
89 detection. Although results of quantitative analyses can vary depending on the metric  
90 employed, not much guidance for researchers is available in the scientific literature on the use  
91 of frontal metrics, the differences between them and factors to consider during their statistical  
92 processing. Considering the complex process of generating frontal maps and metrics, this  
93 represents essential information for users outside the field to ensure best practice and avoid  
94 pitfalls during quantitative analysis.

95

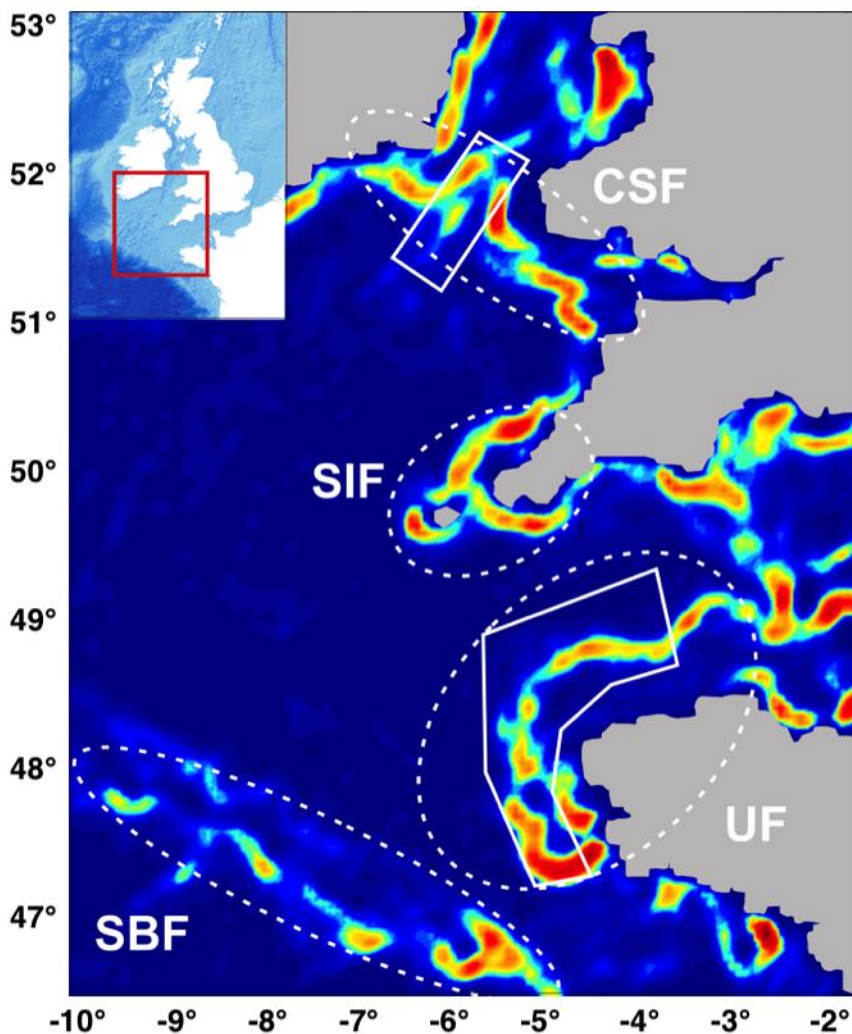
96 There is also a lack of information regarding factors influencing the metrics directly, such as  
97 the quantity of data used to create a frontal map or the effect of spatial averaging over larger  
98 areas in order to create time series. However, it is essential to consider these factors in order  
99 to avoid incorrect estimates of a front. For example, there has been a steep and continuous  
100 increase in satellite passes over the past 20 years, resulting in an increased number of satellite  
101 images per day and therefore, higher data availability, which affects temporal variability  
102 pattern (Oram et al. 2008). Although varying sampling size can affect the results of statistical  
103 analyses, not many studies concerning long-term trends of satellite-derived frontal metrics  
104 account for this (e.g. Belkin et al., 2005; Kahru et al., 2012; Ullman et al., 2007). Some  
105 studies ensure data quality during the processing stage, e.g. only images with at least 90%  
106 cloud-free pixels are used, but do not account for data availability during statistical analysis  
107 (Obenour 2013).

108

109 This paper provides guidance on the use frontal metrics and their quantitative analysis,  
110 particularly directed towards users outside remote frontal detection. We demonstrate the  
111 necessity to account for influencing factors and how to deal with them, including i) a strong  
112 non-linear effect of data availability, ii) bias introduced by not distinguishing between  
113 different frontal types and iii) the choice of metric to be used. We show how these factors  
114 influence the distinct temporal pattern of some commonly used frontal metrics over 20 years

115 from January 1990 to December 2010. The focus of this study are two tidal mixing fronts,  
116 which form in the Celtic Sea during the spring when the water is stratified, namely the Celtic  
117 Sea and Ushant Front. These two fronts separate the Celtic Sea from the Irish Sea and  
118 Western English Channel respectively (Figure 1). Tidal mixing fronts are transition zones  
119 between tidally-mixed coastal and seasonally-stratified shelf waters and are critical in shaping  
120 oceanographic and biological processes during the summer months (LeFevre, 1986; Simpson  
121 and Sharples, 2012). The temporal variability of the Celtic Sea and Ushant Front is well  
122 documented from four decades of *in-situ* and modelling studies (Brown et al., 2003; Elliott et  
123 al., 1991; Holt et al., 2010; Neil et al., 2013; Pingree et al., 1978; Young et al., 2004), which  
124 provide a reference for the results of this research.

125  
126  
127  
128  
129



130

131 **Figure 1 (colour): Frontal density map (June 2009) showing thermal fronts of the Celtic**  
132 **Sea.** Red colours refer to strong and persistent fronts and blue colours to no frontal activity.  
133 The white dotted circles highlight the tidal mixing fronts UF=Ushant Front, SIF=Scilly Isles  
134 Front,CSF=Celtic Sea Front and the shelf break front=SBF. The white polygons refer to the  
135 two sampling areas used in this research (Celtic Sea and Ushant Front). Parametrisation of the  
136 boundary definition for the two front polygons can be found in section 2.4 and in the  
137 supplement.  
138

## 139 2 Methods

### 140 2.1 Processing of frontal maps

141 Frontal maps used in this research are based on Advanced Very High Resolution Radiometer  
142 (AVHRR) data from National Oceanic and Atmospheric Administration (NOAA) satellites.  
143 These raw data were acquired, translated into SST values, geo-corrected, cloud masked, and  
144 mapped at 1.1km<sup>2</sup> resolution by the NERC Observation Data Acquisition and Analysis  
145 Service (NEODAAS) ([www.neodaas.ac.uk/data](http://www.neodaas.ac.uk/data)). Both day and night images were  
146 considered. Fronts were detected on each satellite image by application of the Single Image  
147 Edge Detection algorithm (SIED) developed by Cayula and Cornillon (1992). In this  
148 approach, a histogram of the SST frequency distribution is created, based on a user-defined  
149 array of pixels, but usually 32x32 pixels (also used in this research). If the histogram has a  
150 bimodal form, it suggests the presence of two different water masses. In order to qualify as  
151 two separate water masses, the temperature difference between the two populations has to be  
152 at least 0.4°C as recommended when applied to low-noise SST data (Miller, 2009). The SIED  
153 then marks the transitional values between the two modes of the histogram as *valid* pixels =  
154 frontal (*Fvalid*).  
155

156 A SIED-derived frontal map from a single satellite image is unsuitable for the description of  
157 meso-scale features due to their high spatio-temporal variability and the frequency of cloud  
158 cover in the study region, which disguises dynamic processes (Miller, 2009). Therefore, in  
159 this research we used frontal maps at monthly resolution, which means that all fronts detected  
160 on single SST images during a given month are aggregated into a single map for each metric  
161 as defined below, in order to highlight stable frontal features (Miller, 2009). Although higher  
162 temporal resolution would have been more desirable to investigate seasonal pattern of tidal  
163 mixing fronts, weekly and fortnightly frontal maps were still highly affected by cloud cover  
164 (even during the summer months and particularly at the beginning of the study period in the  
165 early 1990's) and were unsuitable for the analysis. In addition, the resolution of the frontal  
166 maps was scaled down to 4.8km<sup>2</sup> by taking the mean of a four by four pixel array on the final  
167 map. Spatial downscaling was performed to reduce variability around the frontal contours,  
168 which facilitated the determination of the sampling area (see supplementary section 6.1).

169 Further steps of data processing depend on the metric chosen and are explained in detail  
170 below.

171

## 172 **2.2 Frontal metrics used in this research**

173 In the following description, the word image refers to a satellite image of the study area,  
174 which consists of an array of pixels. Maps refer to the satellite images after frontal  
175 algorithms have been applied and show frontal metrics. The example pixel is at a given  
176 location of an image (e.g. uppermost left corner), on a map or over a sequence.

177

178 ***Fclear*** and ***Fvalid***: For each pixel in the monthly map, *Fclear* and *Fvalid* simply provide the  
179 total amount of clear and valid pixels respectively. Valid pixels (*Fvalid*) are pixels that have  
180 been identified by the SIED-algorithm as frontal (described in section 2.1). Clear pixels are  
181 pixels that were not cloud covered and had a clear satellite view on the ocean, whether or not  
182 a front was observed. For example, if 40 images were obtained over the period of one month,  
183 30 of these had clear views on an example pixel, and in the other ten images this pixel was  
184 obscured by clouds, the *Fclear* value for this pixel would be 30. Out of the 30 clear views, if  
185 the example pixel was identified as a front 20 times by the SIED-algorithm, the *Fvalid* would  
186 be 20.

187

188 ***Fprob*** (Figure 2 and **Table 1**) represents the probability of observing a front in a given pixel  
189 over the sequence of images used (Miller, 2009). As in the example above, out of the 30 clear  
190 views, if the example pixel was identified as a front 20 times by the SIED-algorithm, then the  
191 *Fprob* value for this pixel would be:

192

$$193 \quad F_{prob} = \frac{\text{front pixels}}{\text{clear pixels}} = \frac{20}{30} = 0.67.$$

194

195 Frontal (also called valid) and clear pixels are described in more detail further below under  
196 *Fvalid* and *Fclear*. The higher the *Fprob* value, the more often a front was detected in the  
197 pixel. Therefore, clusters of pixels with high *Fprob* on a frontal map represent areas of higher  
198 frontal occurrences. The advantage of *Fprob* is that it is simple and easy to understand.  
199 However, there are two apparent disadvantages. Firstly, it is a proportion and can easily be  
200 biased when the relationship between the numerator and denominator is not linear or if both  
201 change in the same direction, but at different rates. Secondly, *Fprob* does not provide  
202 information on the strength of a front.

203

204 *Fmean* provides information on the temperature gradient (temperature change per pixel) and  
 205 hence, an indication of the strength of a front (Miller, 2009). After applying the SIED-  
 206 algorithm to a single image, the temperature gradients between a front pixel and its  
 207 neighbouring pixels are calculated. The value of the greatest gradient found is assigned to the  
 208 example pixel. This is done for all valid pixels on a map and all images going into a map. For  
 209 the monthly map, the mean of all temperature gradient values is calculated for the example  
 210 pixel. However, the mean is only based on front pixels in the sequence and not on pixels that  
 211 were cloud free but non-frontal as it is the case for *Fprob*. This is in order to avoid degrading  
 212 the metric with gradients not associated with fronts, or with low gradients observed where a  
 213 dynamic front was previously located. Using the same example as above, the temperature  
 214 gradient was calculated for the 20 front observations of the example pixel.:

215

$$216 \quad Fmean = \frac{\text{sum of gradient values (20 different values)}}{\text{total number of frontal pixels}} = (e.g.) \frac{21.4}{20} = 1.07$$

217

218 It should be noted that *Fmean* disregards of clear pixels. On the one hand, this makes  
 219 *Fmean* less sensitive to data availability (*Fclear*) and does lessen the visualisation of  
 220 ephemeral features. On the other hand, it does not distinguish between pixels that were  
 221 identified as frontal frequently versus ones that were not. For instance, the example pixel was  
 222 identified as frontal 20 times in the sequence of 30 clear images and had an *Fmean* of 1.07.  
 223 Another pixel has been identified as frontal twice in the sequence of 30 clear images, but also  
 224 had a temperature gradient of 1.07 each time. This pixel will receive the same value on the  
 225 map as first one although its frontal frequency was very small. This results in maps containing  
 226 many transient frontal segments that are displayed with the same strength as the persistent  
 227 ones, which can introduce noise to a map.

228

229 *Fpers* is the product of multiplying the final (in our case monthly) map of *Fmean* by the final  
 230 map of *Fprob*:

231

$$Fpers_{final} = Fmean_{final} \times Fprob_{final}$$

232

233 By weighting *Fmean* by a measure of persistence (*Fprob*), areas of frequently occurring  
 234 fronts are highlighted and noise introduced by short-lived frontal segments is reduced (Miller,  
 235 2009). While the multiplication of *Fprob* and *Fmean* aids visualisation of more consistent  
 236 features, it complicates interpretation of the metric itself, because it is comprised of two  
 237 entities that have different meanings. A change in *Fpers* cannot be directly attributed to  
 238 either changes in *Fprob* or *Fmean* (or both), whereas it might be crucial to know which

239 metric is more affected, e.g. if interested in the meteorological drivers of the observed  
 240 variability.

241

242 In *Fcomp* maps an additional weighting factor (*Fprox*) is applied to the monthly map of  
 243 *Fpers*, which considers the spatial proximity of frontal pixels (Miller, 2009):

244

$$Fcomp_{final} = Fpers_{final} \times Fprox$$

245

246 Pixels near or in clusters of valid pixels, will receive an additional *boost*. The closer the pixel  
 247 is to a frontal cluster, the more it will be boosted. This process will ignore pixels located  
 248 beyond a certain distance from any frontal clusters. The resulting maps further emphasise  
 249 persistent features and further reduce the occurrence of noise. Like *Fpers*, *Fcomp* obscures  
 250 the influence of each of the components for the final product and it is not possible to identify  
 251 the most variable component.

252

253 *Fdens* is an *Fcomp* map with an additional spatial smoother (in this case a Gaussian filter of  
 254 five pixels width) applied to the final *Fcomp* map in order to turn the discrete front segments  
 255 into a continuously-varying spatial map (Scales et al., 2015). *Fdens* is particularly useful for  
 256 visualisation of persistent, spatially stable features as it removes nearly all transient frontal  
 257 segments:

258

$$Fdens_{final} = Fcomp_{final} \times spatial\ smoother$$

259

260

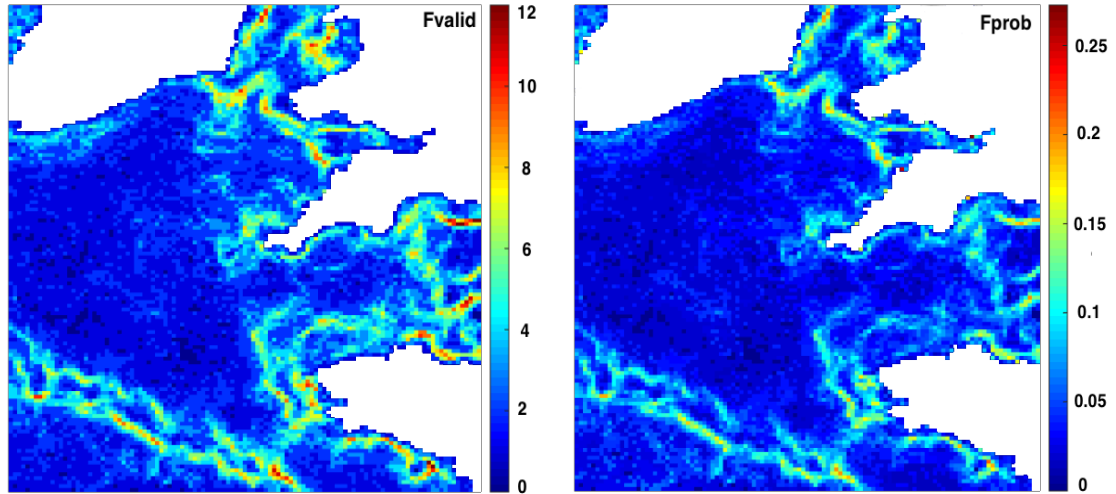
261

262

**Table 1:** List of metrics used in this research and their abbreviations, common names, quantitative derivation, value range and spatio-temporal resolution.

<b>Metric</b>	<b>Common name</b>	<b>Definition</b>	<b>Value range</b>	<b>Spatio-temporal res.</b>
<i>Fvalid</i>	Valid pixels	Total of valid (frontal) pixels in a sequence of images	Any positive integer	Monthly 4.8km <sup>2</sup>
<i>Fclear</i>	Clear pixels	Total of clear pixels in a sequence of images	Any positive integer	Monthly 4.8km <sup>2</sup>
<i>Fprob</i>	Frontal probability	$\frac{Fvalid}{Fclear}$	0-1	Monthly 4.8km <sup>2</sup>

<b><i>Fmean</i></b>	Temperature gradient	$\frac{\text{Temperature gradient}}{F_{\text{valid}}}$	0-2.54	Monthly 4.8km <sup>2</sup>
<b><i>Fpers</i></b>	Frontal persistence	$F_{\text{prob}} \times F_{\text{mean}}$	0-0.254	Monthly 4.8km <sup>2</sup>
<b><i>Fcomp</i></b>	Frontal composite	$F_{\text{pers}} \times F_{\text{prox}}$ <i>Fprox</i> = additional <i>boost</i> , when other frontal clusters in the neighbourhood	0-0.254	Monthly 4.8km <sup>2</sup>
<b><i>Fdens</i></b>	Frontal density	$F_{\text{comp}} + \text{spatial smoother}$	0-0.254	Monthly 4.8km <sup>2</sup>



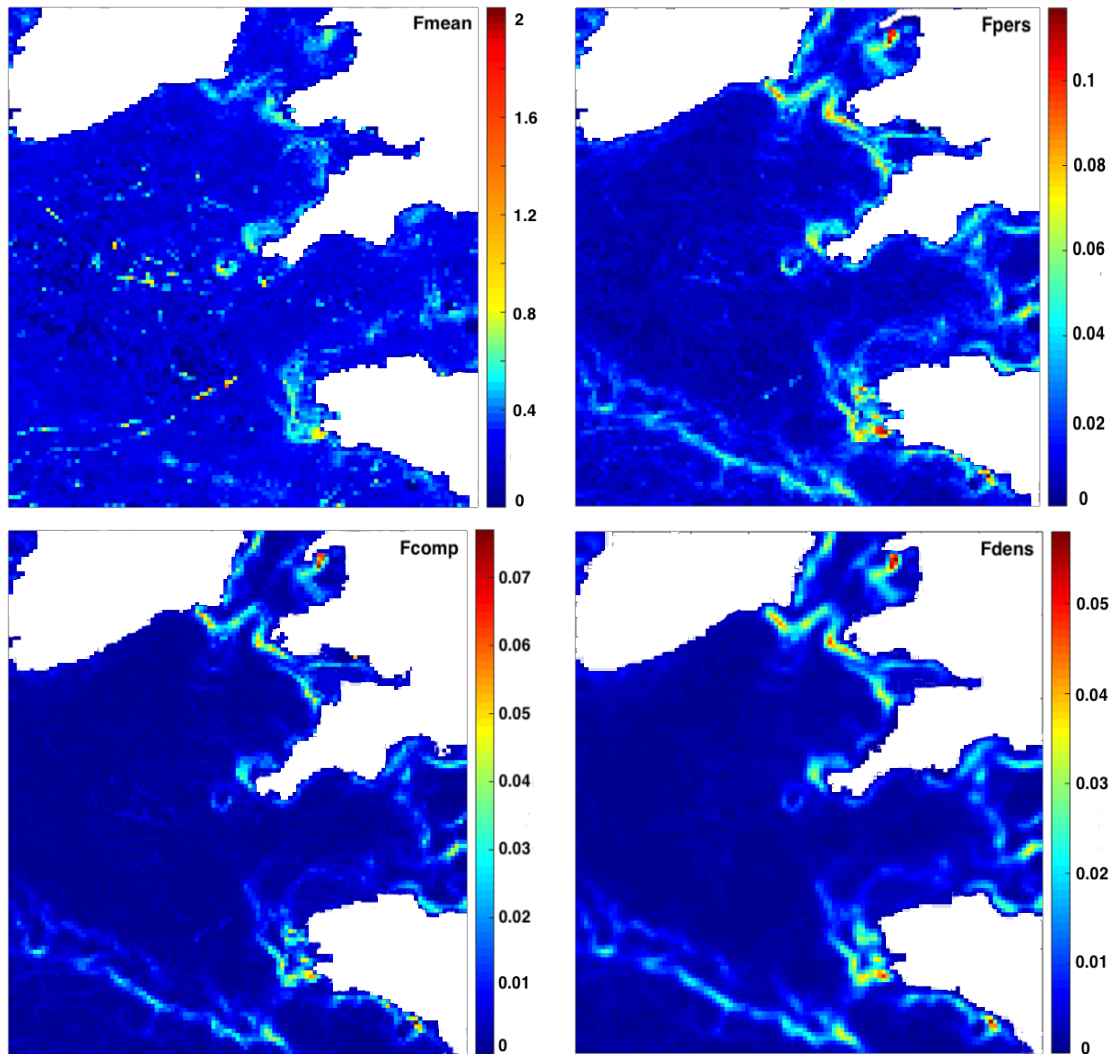


Figure 2 (colour): Monthly maps for  $F_{valid}$ ,  $F_{prob}$ ,  $F_{mean}$ ,  $F_{pers}$ ,  $F_{comp}$  and  $F_{dens}$  from June 2009. Pixels covering land are no-value pixels and therefore, come up as white.

### 263 2.3 Spatial averaging of frontal pixels over the sampling area

264 To investigate inter-annual and seasonal variability of the selected frontal metrics at the Celtic  
 265 Sea and Ushant Front, a time series for each metric shown in figure 2 and  $F_{clear}$  was created.  
 266 For this, all pixels within each of the two frontal areas were spatially averaged to obtain a  
 267 single value per front and monthly map. The position of tidal mixing fronts varies seasonally,  
 268 in response to tidal movements, storm events and other factors. Therefore, the sampling area  
 269 for each front needed to be large enough to capture the spatial variability of the fronts, but  
 270 small enough to exclude unwanted features in the vicinity as much as possible, which could  
 271 bias estimates of the fronts of interest (e.g. other fronts such as river plumes or coastal  
 272 currents). In order to identify a suitable sampling area, core frontal areas were visually  
 273 identified using  $F_{comp}$  maps for the Celtic Sea and Ushant Front. Position and extend of each  
 274 front are known from previous studies (Ref) . Based around the core area different sized  
 275 subsets were created, which were resampled to find the most suitable sampling area and to

276 ensure no bias caused by an *area size effect* was introduced. Details of the resampling  
 277 approach can be found in the supplement (Section 6.1)

278

279 The spatial averaging can either include all pixels (including non-frontal, but clear) or frontal  
 280 pixels only. Since the subjects of interests are fronts, one might consider using frontal pixels  
 281 only, and hence, extract merely information on the fronts. However, using only frontal pixels  
 282 would result in highly variable sampling sizes of the spatial averages, because there will be  
 283 fewer frontal pixels during winter and more during the summer due to the seasonal nature of  
 284 the fronts of interest (Sup.Table 1). In addition, there will be more frontal pixels during  
 285 periods of higher *Fclear* (e.g. the summer months or good weather periods). Sampling size  
 286 can affect the results of statistical analyses. In order to avoid a sample size effect, spatial  
 287 averaging in this research was performed using all pixels, including both front and non-frontal  
 288 pixels.

289

## 290 2.4 Statistical analyses

291 Correlation analyses showed that the metrics *Fprob*, *Fpers*, *Fcomp* were strongly related.  
 292 *Fdens* displayed highest correlations with *Fcomp* and *Fmean* (**Table 2**). Subsequently,  
 293 analyses in this research were conducted on *Fprob* (representative for the group *Fprob*,  
 294 *Fcomp* and *Fpers*) and *Fmean* only. *Fprob* was selected because it is a) more comprehensible  
 295 than other complex metrics, b) frequently used in remote sensing research, and c) the driving  
 296 component in *Fcomp* and *Fpers* in our dataset (although this can differ in other systems).  
 297 *Fmean* has been less frequently used in ecological or oceanographic time series, but is  
 298 included because it provides useful information on the strength of the front and hence, other  
 299 characteristics than *Fprob*. Time series plots of metrics not included in the analysis (*Fpers*,  
 300 *Fcomp* and *Fdens*) can be found in the supplement (Sup. Figure 3 and Sup. Figure 4).

301

**Table 2:** Pearson Product Moment correlation coefficients (*r*) after extraction of the seasonal variability for all metrics combinations. Lower left diagonal (blue font) refers to Celtic Sea Front and upper right diagonal (black font) to Ushant Front correlations. Coefficients above 0.7 are in **bold** and, *italic* numbers are coefficients of correlation analyses with *p-values* <0.05.

Metric/ <i>r</i>	<i>Fprob</i>	<i>Fpers</i>	<i>Fcomp</i>	<i>Fmean</i>	<i>Fdens</i>
<i>Fprob</i>	-	<i>0.9</i>	<i>0.9</i>	-0.04	<i>0.3</i>
<i>Fpers</i>	<i>0.9</i>	-	<i>1.0</i>	<i>0.2</i>	<i>0.5</i>
<i>Fcomp</i>	<i>0.9</i>	<i>1.0</i>	-	<i>0.2</i>	<i>0.6</i>
<i>Fmean</i>	<i>-0.3</i>	<i>0.06</i>	<i>0.06</i>	-	<i>0.6</i>
<i>Fdens</i>	<i>0.3</i>	<i>0.5</i>	<i>0.6</i>	<i>0.6</i>	-

302

303 Inter-annual and seasonal variability of  $F_{prob}$  and  $F_{mean}$  and the effect of  $F_{clear}$  on this  
304 variability were investigated using anomalies. Anomalies for statistical analysis were created  
305 by subtracting the overall mean of the time series from each data point of the time series  
306 (each month-year combination). Temporal explanatory variables were  $year$  to account for  
307 interannual variability,  $month$  to account for seasonal variability and  $F_{clear}$  to account for  
308 variations in data availability. To demonstrate the effect of  $F_{clear}$  on  $F_{prob}$  and  $F_{mean}$ ,  
309 predictions of monthly and yearly variability of the two metrics are shown from two models,  
310 one with and one without the  $F_{clear}$  variable. For visualisation purposes, monthly and yearly  
311 anomalies were calculated by subtracting the overall mean from the mean of each month/year  
312 respectively. For inter-annual variability plots only months March to November were  
313 considered (see below) to avoid the unwanted inclusion of wintertime fronts (present in the  
314 study area) not associated with the tidal mixing fronts.

315

316 Generalized Additive Mixed Models (GAMMs) with an autoregressive correlation structure  
317 of order one (AR(1)) were used in order to account for temporal autocorrelation and the non-  
318 linear relationship between the response and explanatory variables. The GAMMs take the  
319 structure as specified by Hastie and Tibshirani (1987) and were fitted using the *gamm*  
320 function in the *mgcv* package (Wood, 2006). Smoothed terms were fitted as regression splines  
321 with fixed maximum degrees of freedom ( $k=6$ ) for the covariate  $month$  and  $F_{clear}$  in order to  
322 avoid overfitting. The variable  $month$  was modelled using cyclic cubic regression splines,  
323 setting knots manually between 3 (March) and 11 (November) in order to account for the  
324 circular nature of this term. Model selection was conducted using manual stepwise-backwards  
325 selection. Model fit was examined by means of residual analysis. Residual analysis displayed  
326 a few single outliers in the Celtic  $F_{prob}$  model. The outliers were excluded and the model re-  
327 run, which improved model fit, but did not affect significances of the variables.

## 328 **3 Results**

### 329 **3.1 Temporal variability of $F_{mean}$ and $F_{prob}$**

330 Due to the distinct nature of the two metrics, their temporal patterns differed significantly.  
331 Overall,  $F_{mean}$  displayed sinusoidal fluctuations with an initial decrease from 1990 to 1996,  
332 followed by an increase from 1997 to 2010 at both fronts (Figure 3). A notable low in  $F_{mean}$   
333 occurred in 1996 at the Celtic Sea and Ushant Front. In contrast to  $F_{mean}$ ,  $F_{prob}$  anomalies  
334 were positive until 1996 and dropped sharply thereafter at both fronts. Apart from minor  
335 variations, temporal variability of  $F_{prob}$  was consistent for the remainder of the time series.  
336 Extremely high values of  $F_{prob}$  were observed in 1990 and 1996 at the Celtic Sea Front,  
337 which were less pronounced at the Ushant Front. Overall differences between the Celtic Sea

338 and Ushant Front were low for each metric and occurred predominantly in the first ten years  
339 of the time series. In addition, values for both metrics were slightly higher at the Celtic Front  
340 compared to the Ushant Front:  $F_{mean}$  Celtic:  $0.22 \pm 0.09$ , Ushant:  $0.19 \pm 0.08$ ;  $F_{prob}$  Celtic:  
341  $0.078 \pm 0.03$ , Ushant:  $0.072 \pm 0.03$ ).

342

343 There was a fairly consistent increase in  $F_{clear}$  and  $F_{valid}$  from 1990 to 2010 (Figure 3).  
344 Anomalies became positive at both fronts in the middle of the time series, around 2001.  
345 However, since 2005 the trend stagnated and there was even a slight decrease in  $F_{clear}$  and  
346  $F_{valid}$  in the late 2000's. Notable lows in  $F_{clear}$  and  $F_{valid}$  coincided with the low  $F_{mean}$   
347 and high  $F_{prob}$  years of 1990 and 1996. The relationship between the observed increase in  
348  $F_{clear}$  and interannual variability of  $F_{prob}$  and  $F_{mean}$  is described in the following section  
349 3.22.

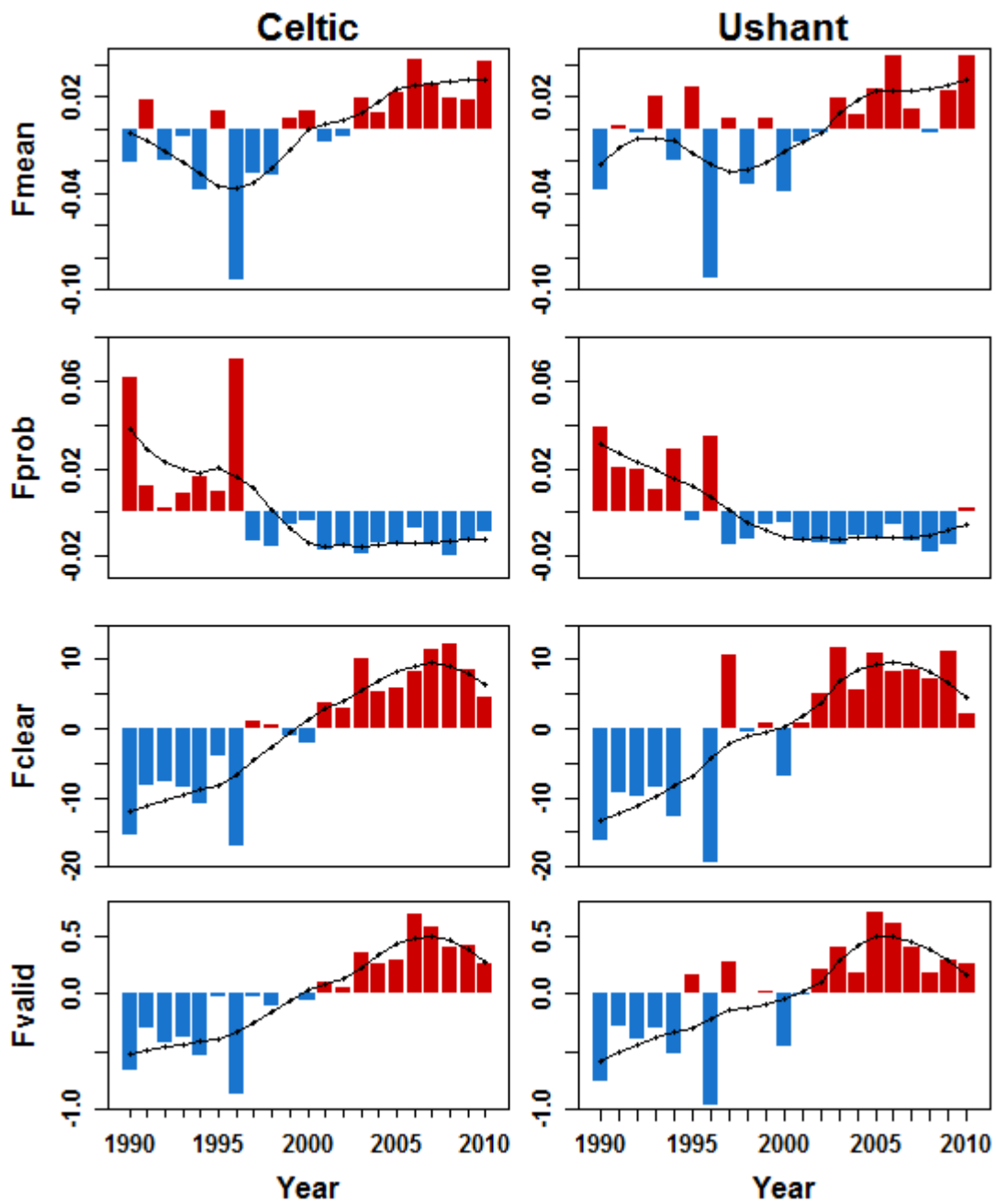
350

351  $F_{mean}$  displayed a typical seasonal curve at both fronts with increasing values from the  
352 beginning of the year until August/September and a sharp decrease thereafter (Figure 4).  
353 Seasonal patterns for  $F_{prob}$  differed between the Celtic Sea and Ushant Front.  $F_{prob}$  values  
354 at the Ushant Front were decreasing until April, became positive in June and did not drop to  
355 negative until December. At the Celtic Sea Front, seasonal fluctuations of  $F_{prob}$  were more  
356 variable. Anomalies were positive during the summer from June to September, negative  
357 between October and November, positive again until February and again negative until June  
358 (Figure 4). The positive  $F_{prob}$  anomalies during the winter months, when tidal mixing fronts  
359 are absent, indicate the inclusion of frontal segments that are not the focus of this study. In  
360 this case, this unwanted signal was likely introduced by parts of a coastal current that runs  
361 along the east coast of Ireland. By restricting the sampling subset to 12km away from the  
362 coasts, it was anticipated to exclude coastal influences, which was clearly not sufficient.

363

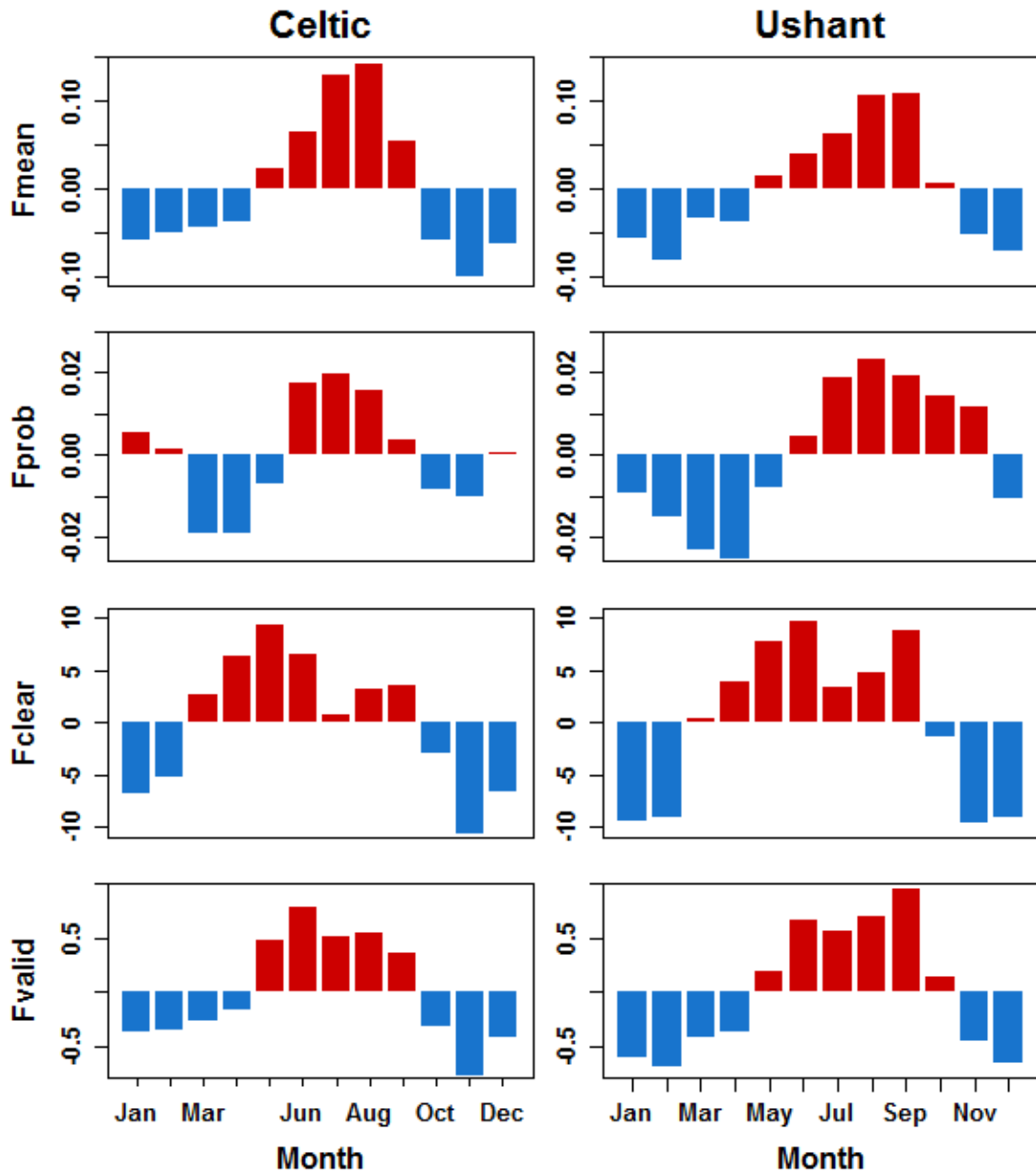
364  $F_{clear}$  and  $F_{valid}$  exhibited typical seasonal cycles, similar to the one seen for  $F_{mean}$  (Figure  
365 4). Positive anomalies of  $F_{valid}$  occurred from May to September at the Celtic Sea Front and  
366 May to October at the Ushant Front. Anomalies of  $F_{clear}$  were positive throughout March to  
367 September at both fronts. However,  $F_{clear}$  values dropped notably in July and increased  
368 slightly again thereafter.

369



370

371 **Figure 3 (colour):** Yearly anomalies of *Fmean*, *Fprob*, *Flclear* and *Fvalid* at the Celtic Sea  
 372 **and Ushant Front from 1990 to 2010.** Anomalies are based on a seasonal subset (March to  
 373 November). Blue bars represent negative anomalies and red positive anomalies. Black line  
 374 represents loess smoother ( $\alpha=0.6$ ).



375

376 **Figure 4 (colour): Monthly anomalies (based on the entire time series) for of  $F_{mean}$ ,**  
 377  **$F_{prob}$ ,  $F_{clear}$  and  $F_{valid}$  at the Celtic Sea and Ushant Front. Blue bars represent negative**  
 378 **anomalies and red positive anomalies.**

379

### 380 **3.2 Effect of $F_{clear}$ on variability of $F_{mean}$ and $F_{prob}$**

381 Preliminary analyses indicated a correlation between  $F_{clear}$  and the two metrics  $F_{prob}$  and  
 382  $F_{mean}$ . The temporal pattern seen for  $F_{prob}$  and  $F_{mean}$  might not purely be a result of  
 383 changes in meteorological or hydrodynamic forcing over seasonal and interannual cycles,  
 384 but caused to a certain degree by variations in available data. To investigate an effect of  
 385  $F_{clear}$  on temporal variability of  $F_{mean}$  and  $F_{prob}$ , inter-annual and seasonal variability of  
 386 both metrics were modelled including  $F_{clear}$  as an explanatory variable. In a follow up

387 analysis, which is not presented here, temporal variability of these fronts was investigated in  
388 relation to meteorological factors known to influence frontal dynamics (e.g. heat flux, wind  
389 speed), but which are also partly correlated with *Fclear* (Suberg, 2015). However, an *Fclear*  
390 effect remained even when accounting for atmospheric forcing and can therefore, not be  
391 explained by covariability with meteorological factors alone. For brevity purposes, this  
392 analysis focuses on *Fclear* only.

393

394 The relationship between *Fclear* and *Fmean* at both fronts was very strong and overall,  
395 positive (Figure 5 and **Table 3**). The relationship was stronger at the lower value range of  
396 *Fclear* and levelled off with increasing *Fclear* (Figure 5). In consequence, accounting for  
397 *Fclear* resulted in changes in the interannual pattern of *Fmean*. The decrease at the beginning  
398 of the time series was stronger and the increase in the second half was less steep compared to  
399 the pattern seen in Figure 3. When *Fclear* was not included in the model, the relationship  
400 between *Fmean* and time was positively linear (Fig. 5, red lines). Although the model fit  
401 should be interpreted with caution as it appears to be an oversimplification of the real  
402 relationship. Not accounting for *Fclear* results generally in a less steep drop at the beginning  
403 of the time series, followed by a stronger increase than. Seasonal variability on the other  
404 hand, was not greatly affected by *Fclear* and still displayed the seasonal cycle and timing as  
405 seen in Figure 4. While factors *Fclear* and *months* explained considerable amount of the  
406 variability, *year* only lead to a 0.03/0.04 (Celtic Sea/Ushant) increase in the model  $R^2$  (**Table**  
407 **3**).

408

409 There was also a significant effect of *Fclear* on *Fprob* (Figure 6 and **Table 3**). In contrast to  
410 *Fmean*, the relationship was negative and levelled off at higher *Fclear* values (Figure 6). The  
411 inclusion of *Fclear* caused a notable modification of the interannual pattern of *Fprob*. The  
412 model accounting for *Fclear* did not suggest significant interannual variability in *Fprob* at the  
413 Celtic Sea and Ushant Front, whereas a model without *Fclear* suggests a negative trend over  
414 time (Figure 6, red lines). In addition, the seasonal curve of *Fprob* was more distinct when  
415 accounting for *Fclear* and showed the expected pattern with higher *Fprob* values in summer  
416 and lower values during the winter, when tidal mixing fronts are absent. A summary of the  
417 effect of *Fclear* on temporal variability of *Fprob* and *Fmean* is given in **Table 4**.

418

419

420

421

422

423

424

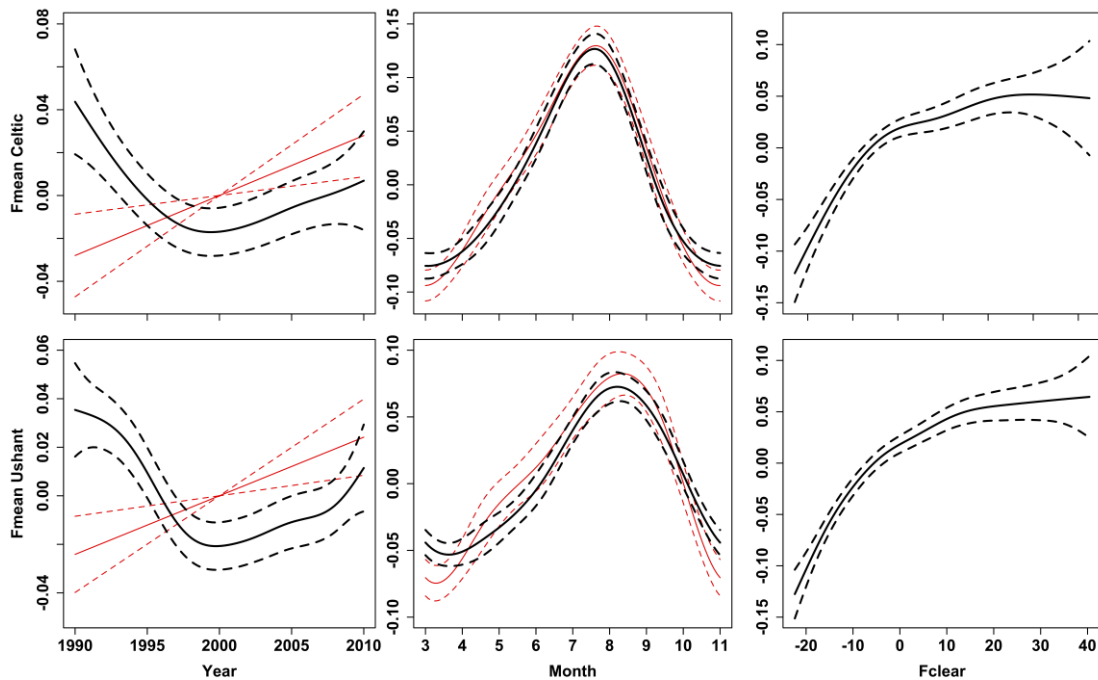
425

426  
427

**Table 3:** Summary of GAMMs with AR1 structure for a seasonal subset of *Fmean* and *Fprob* (March/April to November) anomalies for Celtic Sea and Ushant Front modelled as a function of year, month and *Fclear* (coefficients for model including *Fclear* shown in black, model without *Fclear* shown in red).. Only significant covariates are listed, including their estimated degrees of freedom (edf), F-values, p-values and reduction in AIC. The adjusted R<sup>2</sup> for the final model is given in bold (Adj.R<sup>2</sup>) and increase for each additional variable.

Metric	Front	Covariate (edf)	F-value	p-value	Δ-AIC	Adj. R <sup>2</sup>
<i>Fmean</i>	Celtic	Year (2.77; 1.0)	4.85; 8.5	0.004; 0.004	4.33; 3.6	0.03; 0.03
	Front	Month (3.85; 3.8)	99.96; 68.3	<0.001; <0.001	167.0; 137	0.69; 0.68
		<i>Fclear</i> (4.21)	24.67	<0.001	67.16	<b>0.82</b>
<i>Fprob</i>	Ushant	Year (4.27; 1.0)	4.27; 9.5	<0.001; 0.002	17.54; 4.7	0.04; 0.03
	Front	Month (3.66; 3.7)	67.5; 40.1	<0.001; <0.001	103.82; 86.8	0.53; 0.53
		<i>Fclear</i> (4.26)	47.09	<0.001	111.9	<b>0.78</b>
<i>Fprob</i>	Celtic	Month (3.82; 3.3)	36.1; 10.5	<0.001; <0.001	108.93; 25.6	0.2; 0.2
	Front	<i>Fclear</i> (6.82)	33.65	<0.001	156.98	0.81
		Year (1.4)	13.1	<0.001	11.2	<b>0.4</b>
<i>Fprob</i>	Ushant	Month (3.54; 2.9)	26.03; 7.7	<0.001; <0.001	48.72; 15.7	0.18; 0.2
	Front	<i>Fclear</i> (4.47)	27.58	<0.001	60.05	<b>0.59</b>
		Year (1.9)	10.7	<0.001	11.7	<b>0.4</b>

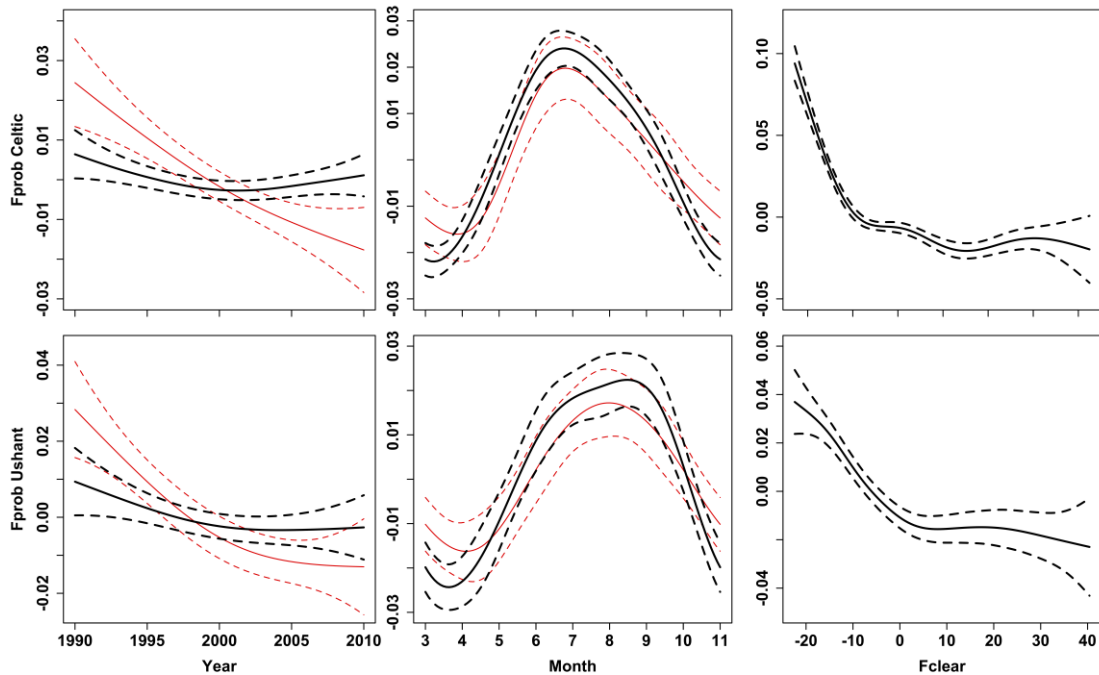
428  
429  
430



431  
432  
433  
434  
435  
436  
437

**Figure 5:** GAMM predictions showing temporal variability (year and month) of *Fmean* anomalies with (black) and without (red) accounting for *Fclear* and the relationship between *Fmean* and *Fclear* at the Celtic Sea Front and Ushant Front. An AR1 structure was added to the GAMM to account for temporal autocorrelation. The model is based on a seasonal subset of *Fmean* (March/April to November,  $N=189/168$ ). Upper panel shows Celtic

438 Sea Front, lower panel Ushant Front. Solid lines represents fitted values, dotted lines 95%  
 439 confidence intervals.  
 440



441  
 442 **Figure 6: GAMM predictions showing temporal variability (year and month) of  $F_{prob}$**   
 443 **anomalies with (black) and without (red) accounting for  $F_{clear}$  and the relationship**  
 444 **between  $F_{prob}$  and  $F_{clear}$ .** An AR1 structure was added to the GAMM to account for  
 445 temporal autocorrelation. The model is based on a seasonal subset of  $F_{prob}$  (March/April to  
 446 November,  $N=189/168$ ). Upper panel shows Celtic Sea Front, lower panel Ushant Front.  
 447 Solid lines represents fitted values, dotted lines 95% confidence intervals. Note: factor “year”  
 448 was insignificant for the inclusive  $F_{clear}$  model (black lines) and is not shown in table 3.  
 449  
 450

**Table 4:** Summary table of the significance of the number of clear pixels and its effect on inter-annual and seasonal variability of  $F_{mean}$  and  $F_{prob}$  at both fronts Celtic Sea and Ushant Front.

Metric	Front	Effect of $F_{clear}$
$F_{mean}$	Celtic Front	Significance: <b>Yes</b> (positive correlation) Inter-annual variability: <b>Strong</b> effect Seasonal variability: <b>Weak</b> effect
	Ushant Front	Significance: <b>Yes</b> (positive correlation) Inter-annual variability: <b>Strong</b> effect Seasonal variability: <b>Weak</b> effect
$F_{prob}$	Celtic Front	Significance: <b>Yes</b> (negative correlation) Inter-annual variability: <b>Strong</b> effect Seasonal variability: <b>Weak</b> effect
	Ushant Front	Significance: <b>Yes</b> (negative correlation) Inter-annual variability: <b>Strong</b> effect Seasonal variability: <b>Weak</b> effect

451  
 452

## 453 4 Discussion

454 This research uses time-series analyses of two seasonal shelf-sea fronts as a framework for  
455 the first coherent guide on the use of satellite-derived frontal metrics in quantitative analyses.  
456 The results of the study will be discussed in the context of managing frontal metrics in  
457 quantitative analyses.

458

### 459 4.1 Recommendations on the choice of metric for temporal analyses

460 Temporal pattern of  $F_{prob}$  and  $F_{mean}$  differed clearly, because they describe two distinct  
461 characteristics of a front; probability versus strength. It is therefore, essential to be clear about  
462 the study hypothesis prior to analysis, and to choose the metric accordingly. Both metrics  
463 appear suitable to study temporal variability of fronts – a result that concurs with previous  
464 research. The seasonal cycles of  $F_{mean}$  and  $F_{prob}$  are in agreement with the onset and  
465 breakdown of stratification in the Celtic Sea and previous observations of the Celtic Sea and  
466 Ushant Fronts (Eliot and Clarke, 1991; Pingree, 1975; Young et al., 2004). Model simulations  
467 of stratification in the Celtic Sea predict the thermocline to establish around the Celtic Deep  
468 first (near the Celtic Sea Front) around April, advancing over the shelf and reaching the  
469 Western English Channel (location Ushant Front) within a month. The delay in frontal  
470 development between the Ushant and Celtic Sea Front was also indicated by the satellite data  
471 (Figure 4, 5 and 6).

472 The results of the long-term analysis suggest that the strength of the frontal temperature  
473 gradient oscillated between 1990 and 2010 at both fronts (Figure 5 and 6). Oscillations in  
474 frontal strength are expected in response to meteorological forcing (Holt et al, 2010). In a  
475 follow up analysis, which investigates the underlying drivers of the observed temporal  
476 variability, SST and net heat flux were found to be the predominant meteorological factors  
477 explaining the variation in  $F_{mean}$  (Suberg, 2015). An increase in SST in the study area could  
478 have caused the observed intensification of  $F_{mean}$  over the later ten years of the time series.  
479 This is in accordance with modelling studies, predicting tidal mixing fronts in the Celtic Sea  
480 to intensify due to increasing water temperatures during this century (Holt et al, 2010; Marsh  
481 et al., 2015). Inter-annual pattern of  $F_{prob}$  showed abnormally high values (and low values in  
482  $F_{mean}$ ) in 1990 and 1996. These extremes are partially caused by confounding factors, such  
483 as higher than usual cloud cover, which led to a reduction of available satellite imagery. Other  
484 explanations will be discussed in the next section (4.2). Apart from these extremes, no  
485 obvious changes in  $F_{prob}$  occurred over the study period.

486

487  $F_{comp}$ ,  $F_{pers}$  or  $F_{dens}$  were not analysed in detail here to their high correlation with  $F_{prob}$   
488 and/or  $F_{mean}$ . This is essentially due to the fact that  $F_{prob}$  and  $F_{mean}$  are base metrics for

489 describing frontal characteristics and all other metrics are derivatives of either one or both. In  
490 general, we recommend the use of  $F_{mean}$  or  $F_{prob}$  for temporal analysis over  $F_{comp}$ ,  $F_{pers}$   
491 or  $F_{dens}$ , because the later complicate interpretation without providing additional  
492 information. In spatial analysis on the other hand, complex metrics like  $F_{dens}$  or  $F_{comp}$   
493 provide advantages as they allow for clearer distinction between low and high frontal  
494 frequency areas. Spatial differences between the metrics can be seen in Figure 2. As  
495 mentioned earlier, the choice of metric needs to be well thought through and may differ  
496 depending on spatial or temporal analyses.

497  
498  
499

#### 500 **4.2 Effect of data availability on variability of frontal metrics**

501  $F_{clear}$  had significant, but contrasting effects on the temporal pattern of  $F_{mean}$  and  $F_{prob}$ .  
502 Overall, the relationship between  $F_{clear}$  and  $F_{mean}$  was positive, but levelled out at high  
503 numbers of clear pixels. More clear pixels will lead to more cloud free scenes and  
504 subsequently, a higher detection rate of frontal segments. In addition, indirect factors increase  
505 the relationship between  $F_{mean}$  and  $F_{clear}$ . Stronger temperature gradients across tidal  
506 mixing fronts are likely to be correlated with summer months or good weather periods with  
507 less cloud cover, stronger solar irradiance and higher temperatures. Under these conditions,  
508 tidal mixing fronts will strengthen or develop quicker (Holt et al., 2010; Young et al., 2004).  
509 At the same time, summer months and decreased cloud cover are also linked to higher  $F_{clear}$ .  
510 Therefore, it is essential to account for data availability when using  $F_{mean}$  for quantitative  
511 analyses.  $F_{mean}$  has not been widely used in time series analysis and comparisons with other  
512 studies are not possible.

513

514 In contrast to  $F_{mean}$ , the relationship between  $F_{prob}$  and  $F_{clear}$  in the lower value ranges was  
515 negative. The reason for the negative correlation is that  $F_{prob}$  is a simple proportion between  
516 valid and clear pixels ( $F_{valid}$  and  $F_{clear}$ ). There was a strong positive correlation between  
517  $F_{valid}$  and  $F_{clear}$  ( $r=0.8$ ) and a notable increase over time for both. In addition, years with  
518 notably low  $F_{clear}$ , and for that matter low  $F_{valid}$  (e.g. 1990 and 1996), showed  
519 disproportionately high  $F_{prob}$  values. This contradictory pattern is due to a *divisor* effect. Over  
520 the time frame of this research, the increase in number of satellites has led to an increase in  
521 the number of clear pixels ( $F_{clear}$ ), which was much higher than the increase in the number  
522 of front pixels ( $F_{valid}$ ). For example, from the first five years of the time series (1990-1994)  
523 the average number of front pixels in a given location (pixel) increased from  $0.97 \pm 0.42$  to  
524  $1.91 \pm 0.86$  in the last five years (1996-2010) at the Celtic Sea Front (Ushant: from  $0.88 \pm 0.45$

525 to  $1.56 \pm 0.9$ ), whereas clear pixels have risen from  $11.62 \pm 6.15$  to  $30.75 \pm 13.38$  (Ushant:  
526 from  $10.7 \pm 6.55$  to  $27.28 \pm 15.22$ ). This represents a 2.65-fold increase in clear pixels (Ushant:  
527 2.55), but only a 1.97-fold increase in front pixels (Ushant: 1.77). Therefore, the number of  
528 front pixels is divided by an increasingly higher number of clear pixels over time, which  
529 results in a decrease of  $F_{prob}$  ( $F_{prob} = F_{valid}/F_{clear}$ ). The average  $F_{prob}$  for 1990-1994 was  
530 0.08 compared to 0.06 between 2006 and 2010 at both fronts. According to this, frontal  
531 probability has decreased by 25% from the first to the last quarter of the time series, which is  
532 unlikely and not supported by any other studies concerning interannual variability of  $F_{prob}$   
533 (e.g. Belkin et al., 2005; Kahru et al., 2012).

534

535 The  $F_{clear}$  effect also adds to the high  $F_{prob}$  values observed during winter. Tidal mixing  
536 fronts are absent during this time of the year and the high  $F_{prob}$  indicates, on the one hand,  
537 the inclusion of signals from wintertime fronts, which will be discussed in section 4.3.  
538 However, the signal was much lower in  $F_{mean}$ . It is likely that higher cloud cover during  
539 winter leads to fewer clear pixels and hence,  $F_{valid}$  being divided by a smaller number of  
540  $F_{clear}$ , which resulted in an elevated  $F_{prob}$ , while  $F_{mean}$  was not affected by the divisor  
541 effect.

542

543 The relationship between  $F_{prob}$  and  $F_{clear}$  has largely been ignored in the majority of  
544 research that uses satellite imagery to investigate temporal variability of fronts (e.g. Belkin et  
545 al., 2005; Kahru et al., 2012) and only been mentioned in a couple of studies (Obenour, 2013;  
546 Oram et al. 2008; Ullman et al., 2007). Oram et al. 2008 note that the increase in available  
547 satellite images during the second half of their study (1997-2002) caused bias in their  
548 detection probabilities ( $F_{prob}$ ). Ullman et al. (2007) suggested that the non-linear relationship  
549 between clear and front pixels is caused by the failure of the SIED-algorithm to identify all  
550 frontal pixels as such, particularly in partially cloud-covered scenes. The clouds block the  
551 contour-following part of the SIED algorithm, resulting in  $F_{prob}$  being underestimated.  
552 Obenour (2013) suggests the SIED-window should be at least 90% cloud-free during image  
553 processing in order to avoid exactly this problem and subsequently, avoid temporal variability  
554 of  $F_{prob}$  caused by the fraction of clear pixels. Obenour (2013) addresses the  $F_{clear}$  effect by  
555 increasing data quality at the expense of data quantity: that approach differs to the one used in  
556 this study, which accounts for the amount of clear pixels during the statistical analysis stage,  
557 regardless of the difficulties caused by partially cloudy scenes.

558

559 Most temporal variability studies focus on seasonal variability and did not report any  
560 discontinuities of  $F_{prob}$  caused by  $F_{clear}$  (e.g. Castelao et al., 2014; Hickox et al., 2000;  
561 Mavor et al., 2001). However, the  $F_{clear}$  effect appears to be less obvious when investigating

562 seasonal variability, as seen in this study. Less research has focused on interannual patterns  
563 and mostly reported an increase in *Fprob* over time. For example, Belkin and Cornillon  
564 (2005) found a surprising 50% rise in the annual mean of *Fprob* between 1985-96, averaged  
565 over the entire Bering Sea. Similarly, Kahru et al. (2012) showed a significant increase in  
566 *Fprob* in the California Current System over 29 years (1981-2009). However, both studies did  
567 not consider the changes in available data. Ullman et al. (2007) used frontal maps from 1985  
568 to 2001 to investigate temporal and spatial variability of *Fprob* in four regions of the North  
569 Atlantic. They mentioned the dependency of *Fprob* on *Fclear*, which could lead to an  
570 underestimation of *Fprob*. However, they concluded that it did not influence their results,  
571 because seasonal peaks of *Fclear* did not coincide with peaks in *Fprob*. In this research the  
572 seasonal pattern between *Fprob* and *Fclear* were not identical either, showing different  
573 seasonal peaks, but the relationship became evident only during the modelling process.  
574 Therefore, Ullman et al. (2007) might have underestimated the effect of *Fclear*. Obenour  
575 (2013) is the only study to our knowledge that accounts for the clear pixel issue in their  
576 analyses, using the method described above (SIED-window >90% cloud free). Despite  
577 accounting for *Fclear*, Obenour (2013) still found an overall increase in global *Fprob* from  
578 1981 to 2011, which varied between different (selected) regions of the world.

579

580 Although most of these studies did not account for *Fclear*, they generally report a rise in  
581 *Fprob* over time. Direct comparisons between this study and previous research are difficult,  
582 because of different study locations (e.g. California Current System, Bering Sea), study  
583 periods and durations, and the fact that these studies combine distinct fronts by spatially  
584 averaging over large areas. Subsequently, winter and summer time fronts, which may have  
585 different long-term trend pattern, are merged. For example, Belkin and Cornillon (2005) use  
586 frontal maps from before 1995, a period when the increase in satellite imagery was not as  
587 marked. It is possible that a *divisor* effect in other parts of the world is not as significant  
588 because of different weather patterns and cloud cover throughout the year. It is also possible  
589 that in this research the effect of *Fclear* has been overestimated by the statistical model,  
590 masking genuine temporal variability in the other metrics.

591

592 In summary, the effect of *Fclear* on *Fmean* and *Fprob* is strong and the amount of available  
593 data should always be considered in any analysis. Because of the non-linear relationship  
594 between *Fclear* and *Fprob/Fmean*, not all variability will be removed when accounting for  
595 *Fclear* and variability relating to actual changes in frontal occurrence can still be observed. In  
596 addition, *Fclear* is mostly an issue in the lower value ranges. Therefore, one could use data  
597 above a certain *Fclear* threshold only (determined via statistical analysis on the given dataset)  
598 and make the assumption that all the variability observed is actually due to changes in the

599 **frontal structure**. It clearly requires more investigations on how to best account for an *Fclear*  
600 effect. A combined approach appears sensible, whereby an *Fclear* effect is reduced during  
601 frontal map processing (Obenour, 2013) and subsequently, tested for during statistical  
602 analysis (this research).

603

### 604 **4.3 Importance of differentiating between distinct types of fronts**

605 High values of *Fprob* were found during winter at the Celtic Sea Front, which were likely  
606 frontal segments not belonging to the front of interest, but to a coastal current. The inclusion  
607 of this signal affects the results of temporal analyses, because it adds variability independent  
608 of the front of interest. Different types of fronts respond to atmospheric and hydrodynamic  
609 forcing in specific ways and subsequently, display a distinct spatio-temporal variability  
610 (Hickox et al., 2000). When summarising frontal activity over large areas, e.g. entire seas,  
611 fronts with different temporal variability pattern will be combined and their individual  
612 temporal signals blurred. Therefore, it is difficult to draw meaningful conclusions about  
613 frontal activity from a cumulative temporal signal obtained over large areas.

614

615 It would make sense for any type of temporal analyses, seasonal or trend, to separate distinct  
616 types of fronts. In addition, individual fronts or particular types often play a specific role in  
617 oceanographic or biological processes and their effect on the ecosystem can vary (Scales et  
618 al., 2014). It is therefore of interest for ecologists and oceanographers alike to be able to  
619 distinguish between individual features and study them in isolation. Isolating features of  
620 interest is difficult, particularly in areas with high frontal activity, where various fronts exist  
621 in close proximity and often merge, such as shelf-seas (Achta et al 2015). In this research, the  
622 study area was refined by resampling different sized subsets (see supplement 6.1). Although  
623 the process was parameterized as much as possible, there is some arbitrariness and the  
624 possibility of unwanted features entering the study region. A newly developed technique,  
625 called synoptic front maps, could prove useful for isolating fronts for analysis. It is based on a  
626 novel line-clustering algorithm, which first involves smoothing the *Fmean* map with a  
627 Gaussian, then the most prominent frontal observations and directions are identified and  
628 followed to generate contiguous contours. This front simplification algorithm is in preparation  
629 for publication (Miller, in preparation).

630

631

632

633

## 634 5 Conclusions

635 Frontal maps were initially developed to visualise fronts, using image processing algorithms  
636 to detect, identify and enhance frontal features. However, for statistical analysis the user  
637 should be aware of their qualities and limitations. This guide on frontal metrics highlights  
638 essential points to think about before and during the analysis stage. Metrics belonging to the  
639 group *Fprob*, *Fpers*, *Fcomp* were highly correlated, whereas *Fmean* and *Fdens* displayed  
640 weaker correlations with other metrics. We recommend using *Fprob* for temporal analysis of  
641 frontal persistence and *Fmean* for frontal strength; the more complex metrics hinder  
642 interpretation without adding information. However, for visual analysis, frontal maps based  
643 on complex metrics (e.g. *Fdens*, *Fcomp*) may be more appropriate, because they highlight  
644 persistent features and suppress transient segments that add noise to the maps. Although this  
645 appears to make the use of complex metrics in spatial analysis more desirable, e.g. in ecology  
646 to explain animal distribution, we still recommend the use of interpretable metrics such as  
647 *Fprob* and *Fmean*. Alternatively, a combination of metrics (complex, but spatially clean  
648 versus simple and noisy, but interpretable) can be used to entangle the relationship between  
649 fronts and animal distribution. Secondly, data availability has to be accounted for as it can  
650 introduce spurious trends: *Fprob* and *Fmean* were strongly affected by *Fclear*. A combination  
651 of improving data quality during the data processing stage as well as including *Fclear* as a  
652 factor in statistical models is recommended. We used frontal maps at monthly resolution and  
653 focused on a specific type of front in this research. It would be useful to investigate the *Fclear*  
654 effect on fronts in other regions, on other types of fronts and at higher temporal resolutions.  
655 For example, frontal types other than tidal mixing fronts, which are not subject to  
656 meteorological factors (which tends to covary with *Fclear*) as much could be less sensitive to  
657 *Fclear*. Finally, depending on the research question, scientists should consider studying  
658 individual fronts in isolation to avoid blurring of signals due to contrasting temporal food  
659 prints of different frontal types.

660

## 661 6 Acknowledgements

662 We thank the University of Southampton for financial support of this research and  
663 NEODAAS for acquisition and processing of the satellite data. We are also grateful for  
664 advice and comments from scientists in the Physical Oceanography group of the University of  
665 Plymouth and Dr. Claire Embling and Dr. Simon Ingram from the Plymouth Marine Science  
666 Department.

667

668 **7 References**

- 669 Acha, E. M., Piola, A., Iribarne, O., & Mianzan, H. (2015). *Ecological Processes at Marine*  
670 *Fronts: Oases in the Ocean*: Springer.
- 671
- 672 Alemany, D., Acha, E. M., & Iribarne, O. (2009). The relationship between marine fronts and  
673 fish diversity in the Patagonian Shelf Large Marine Ecosystem. *Journal of*  
674 *Biogeography*, 36(11), 2111-2124. doi: 10.1111/j.1365-2699.2009.02148.x
- 675
- 676 Armstrong, E. M., Wagner, G., Vazquez-Cuervo, J., & Chin, T. M. (2012). Comparisons of  
677 regional satellite sea surface temperature gradients derived from MODIS and  
678 AVHRR sensors. *International Journal of Remote Sensing*, 33(21), 6639-6651. doi:  
679 10.1080/01431161.2012.692832
- 680
- 681 Bauer, R. K., Fromentin, J. M., Demarcq, H., Brisset, B., & Bonhommeau, S. (2015). Co  
682 occurrence and habitat use of fin whales, striped dolphins and Atlantic Bluefin tuna in  
683 the Northwestern Mediterranean Sea. *PloS one*, 10(10), e0139218.
- 684
- 685 Belkin, I. M., & Cornillon, P. (2003). SST fronts of the Pacific coastal and marginal seas.  
686 *Pacific Oceanography*, 1(2), 90-113.
- 687
- 688 Belkin, I. M., & Cornillon, P. C. (2005). Bering Sea thermal front from Pathfinder data:  
689 Seasonal and interannual variability. *Pacific Oceanography*, 2(3-4), 6-20.
- 690
- 691 Belkin, I. M., Cornillon, P. C., & Sherman, K. (2009). Fronts in Large Marine Ecosystems.  
692 *Progress in Oceanography*, 81(1-4), 223-236. doi: 10.1016/j.pcean.2009.04.015
- 693
- 694
- 695 Brodie, S., Hobday, A. J., Smith, J. A., Everett, J. D., Taylor, M. D., Gray, C. A., & Suthers,  
696 I. M. (2015). Modelling the oceanic habitats of two pelagic species using recreational  
697 fisheries data. *Fisheries oceanography*, 24(5), 463-477.
- 698
- 699 Brown, J., Carrillo, L., Fernand, L., Horsburgh, K. J., Hill, A. E., Young, E. F., & Medler, K.  
700 J. (2003). Observations of the physical structure and seasonal jet-like circulation of  
701 the Celtic Sea and St. George's Channel of the Irish Sea. *Continental Shelf Research*,  
702 23(6), 533-561. doi: 10.1016/s0278-4343(03)00008-6
- 703
- 704 Castelao, R. M., & Wang, Y. T. (2014). Wind-driven variability in sea surface temperature  
705 front distribution in the California Current System. *Journal of Geophysical Research-*  
706 *Oceans*, 119(3), 1861-1875.
- 707
- 708 Cayula, J. F., & Cornillon, P. (1992). Edge-detection algorithm for SST images. *Journal of*  
709 *Atmospheric and Oceanic Technology*, 9(1), 67-80. doi: 10.1175/1520-  
710 0426(1992)009<0067:edafsi>2.0.co;2
- 711 Cox, S. L., Witt, M. J., Embling, C. B., Godley, B. J., Hosegood, P. J., Miller, P. I. & Ingram,  
712 S. N. (2017). Temporal patterns in habitat use by small cetaceans at an  
713 oceanographically dynamic marine renewable energy test site in the Celtic Sea. *Deep*  
714 *Sea Research Part II: Topical Studies in Oceanography*, 141, 178-190.
- 715
- 716 Cyr, F., & Larouche, P. (2015). Thermal Fronts Atlas of Canadian Coastal Waters.  
717 *Atmosphere-Ocean*, 53(2), 212-236. doi: 10.1080/07055900.2014.986710
- 718

719 Defra. (2009). Guidance note on "Selection and designation of Marine Conservation Zones"  
720 (Note 1). *Published by the Department for Environment, Food and Rural Affairs.*  
721

722 Defra. (2012). "Marine Strategy Framework Directive Consultation: UK initial assessment  
723 and proposals for Good Environmental Status": London: Department for  
724 Environment, Food and Rural Affairs.  
725  
726

727 Doniol-Valcroze, T., Berteaux, D., Larouche, P., & Sears, R. (2007). Influence of thermal  
728 fronts on habitat selection by four rorqual whale species in the Gulf of St. Lawrence.  
729 *Marine Ecology-Progress Series*, 335, 207-216.  
730

731 Edwards, E. W. J., Quinn, L. R., Wakefield, E. D., Miller, P. I., & Thompson, P. M. (2013).  
732 Tracking a northern fulmar from a Scottish nesting site to the Charlie-Gibbs Fracture  
733 Zone: Evidence of linkage between coastal breeding seabirds and Mid-Atlantic Ridge  
734 feeding sites. *Deep-Sea Research Part II-Topical Studies in Oceanography*, 98, 438-  
735 444. doi: 10.1016/j.dsr2.2013.04.011  
736

737 Elliott, A. J., & Clarke, T. (1991). Seasonal stratification in the Northwest European shelf-  
738 seas. *Continental Shelf Research*, 11(5), 467-492. doi: 10.1016/0278-4343(91)90054-  
739 a  
740

741 European Union. (2008). Directive 2008/56/EC of the European Parliament and the Council  
742 of 17 June 2008. Establishing a framework for community action in the field of  
743 marine environmental policy (Marine Strategy Framework Directive). . *Official*  
744 *Journal of the European Union*, L164, 19-40.  
745

746 Goold, J. C. (1998). Acoustic assessment of populations of common dolphin off the west  
747 Wales coast, with perspectives from satellite infrared imagery. *Journal of the Marine*  
748 *Biological Association of the United Kingdom*, 78(4), 1353-1368.  
749

750 Hastie, T., & Tibshirani, R. (1987). Generalized additive models- Some applications. *Journal*  
751 *of the American Statistical Association*, 82(398), 371-386. doi: 10.2307/2289439  
752

753 Hickox, R., Belkin, I., Cornillon, P., & Shan, Z. (2000). Climatology and seasonal variability  
754 of ocean fronts in the east China, Yellow and Bohai Seas from satellite SST data.  
755 *Geophysical Research Letters*, 27(18), 2945-2948. doi: 10.1029/1999gl011223  
756

757 Holt, J., & Umlauf, L. (2008). Modelling the tidal mixing fronts and seasonal stratification of  
758 the Northwest European Continental shelf. *Continental Shelf Research*, 28(7), 887-  
759 903. doi: 10.1016/j.csr.2008.01.012  
760

761 Holt, J., Wakelin, S., Lowe, J., & Tinker, J. (2010). The potential impacts of climate change  
762 on the hydrography of the northwest European continental shelf. *Progress in*  
763 *Oceanography*, 86(3-4), 361-379. doi: 10.1016/j.pocean.2010.05.003  
764

765 Hopkins, J., Shaw, A. G. P., & Challenor, P. (2010). The Southland front, New Zealand:  
766 variability and ENSO correlations. *Continental Shelf Research*, 30(14), 1535-1548  
767

768 Horsburgh, K. J., Hill, A. E., & Brown, J. (1998). A summer jet in the St George's Channel of  
769 the Irish Sea. *Estuarine Coastal and Shelf Science*, 47(3), 285-294. doi:  
770 10.1006/ecss.1998.0354  
771

772 Hyrenbach, K. D., Forney, K. A., & Dayton, P. K. (2000). Marine protected areas and ocean  
773 basin management. *Aquatic conservation: marine and freshwater ecosystems*, 10(6),  
774 437-458.  
775

776 Kahru, M., Di Lorenzo, E., Manzano-Sarabia, M., & Mitchell, B. G. (2012). Spatial and  
777 temporal statistics of sea surface temperature and chlorophyll fronts in the California  
778 Current. *Journal of Plankton Research*, 34(9), 749-760. doi: 10.1093/plankt/fbs010  
779

780 Le Boyer, A., Cambon, G., Daniault, N., Herbette, S., Le Cann, B., Marie, L., & Morin, P.  
781 (2009). Observations of the Ushant tidal front in September 2007. *Continental Shelf  
782 Research*, 29(8), 1026-1037. doi: 10.1016/j.csr.2008.12.020  
783

784 Lee, M. A., Chang, Y., & Shimada, T. (2015). Seasonal evolution of fine-scale sea surface  
785 temperature fronts in the East China Sea. *Deep-Sea Research Part II-Topical Studies  
786 in Oceanography*, 119, 20-29. doi: 10.1016/j.dsr2.2014.03.021  
787

788 LeFevre, J. (1986). Aspects of the biology of frontal systems. *Advances in Marine Biology*,  
789 23, 163-299.  
790

791 Marsh, R., Hickman, A. E., & Sharples, J. (2015). S2P3-R (v1.0): a framework for efficient  
792 regional modelling of physical and biological structures and processes in shelf-seas.  
793 *Geoscientific Model Development*, 8(10), 3163-3178. doi: 10.5194/gmd-8-3163-2015  
794

795 Mavor, T. P., & Bisagni, J. J. (2001). Seasonal variability of sea-surface temperature fronts on  
796 Georges Bank. *Deep-Sea Research Part II-Topical Studies in Oceanography*, 48(1-3),  
797 215-243. doi: 10.1016/s0967-0645(00)00120-x  
798

799 McClatchie, S., Cowen, R., Nieto, K., Greer, A., Luo, J. Y., Guigand, C., ... & Rudnick, D.  
800 (2012). Resolution of fine biological structure including small narcomedusae across a  
801 front in the Southern California Bight. *Journal of Geophysical Research: Oceans*,  
802 117(C4)  
803

804 Miller, P. (2009). Composite front maps for improved visibility of dynamic sea-surface  
805 features on cloudy SeaWiFS and AVHRR data. *Journal of Marine Systems*, 78(3),  
806 327-336. doi: 10.1016/j.jmarsys.2008.11.019  
807

808 Miller, P. I. (in preparation). A line clustering algorithm with application to simplifying ocean  
809 front maps derived from satellite data. . *Remote Sensing of Environment*.  
810

811 Miller, P. I., Scales, K. L., Ingram, S. N., Southall, E. J., & Sims, D. W. (2015). Data from:  
812 Basking sharks and oceanographic fronts: quantifying associations in the north-east  
813 Atlantic. *Dryad*. doi: <http://dx.doi.org/10.5061/dryad.d0h7s>  
814

815 Munk, P., Fox, C. J., Bolle, L. J., van Damme, C. J. G., Fossum, P., & Kraus, G. (2009).  
816 Spawning of North Sea fishes linked to hydrographic features. *Fisheries  
817 Oceanography*, 18(6), 458-469. doi: 10.1111/j.1365-2419.2009.00525.x  
818

819

820 Neil, C., Cunningham, A., McKee, D., & Polton, J. A. (2012). Remote sensing of seasonal  
821 stratification dynamics in the southern Irish Sea. *Remote Sensing of Environment*,  
822 127, 288-297. doi: 10.1016/j.rse.2012.09.010  
823

824 Nieblas, A. E., Demarcq, H., Drushka, K., Sloyan, B., & Bonhommeau, S. (2014). Front

825 variability and surface ocean features of the presumed southern bluefin tuna  
826 spawning grounds in the tropical southeast Indian Ocean. *Deep Sea Research Part II:*  
827 *Topical Studies in Oceanography*, 107, 64-76.  
828

829 Nieto, K., Demarcq, H., & McClatchie, S. (2012). Mesoscale frontal structures in the Canary  
830 Upwelling System: New front and filament detection algorithms applied to spatial  
831 and temporal patterns. *Remote Sensing of Environment*, 123, 339-346.  
832

833 Obenour, K. M. (2013). *Temporal trends in global sea surface temperature fronts* (Master's  
834 Thesis). Retrieved from <http://digitalcommons.uri.edu/theses/136> (Paper 136)  
835

836 Oram, J. J., McWilliams, J. C., & Stolzenbach, K. D. (2008). Gradient-based edge detection  
837 and feature classification of sea-surface images of the Southern California Bight.  
838 *Remote Sensing of Environment*, 112(5), 2397-2415.  
839

840

841 Owen, R. (Ed.). (1981). Fronts and Eddies in the Sea: mechanisms, interactions and  
842 biological effects. *Analysis of marine ecosystems*, 197-233. New York: Academic  
843 Press.  
844

845 Park, K. A., Ullman, D. S., Kim, K., Chung, J. Y., & Kim, K. R. (2007). Spatial and temporal  
846 variability of satellite-observed subpolar front in the East/Japan Sea. *Deep Sea*  
847 *Research Part I: Oceanographic Research Papers*, 54(4), 453-470  
848

849 Pemberton, K., Rees, A. P., Miller, P. I., Raine, R., & Joint, I. (2004). The influence of water  
850 body characteristics on phytoplankton diversity and production in the Celtic Sea.  
851 *Continental Shelf Research*, 24(17), 2011-2028. doi: 10.1016/j.csr.2004.07.003  
852

853 Peng, R. D. (2008). R package 'simpleboot': Simple Bootstrap Routines (version 1.1-3).  
854

855 Pingree, R. D. (1975). Advance and retreat of the thermocline on the continental shelf.  
856 *Journal of the Marine Biological Association of the United Kingdom*, 55(4), 965-974.  
857

858 Pingree, R. D., & Griffiths, D. K. (1978). Tidal fronts on shelf-seas around British Isles.  
859 *Journal of Geophysical Research-Oceans and Atmospheres*, 83(NC9), 4615-4622.  
860

861 Pirota, E., Thompson, P. M., Miller, P. I., Brookes, K. L., Cheney, B., Barton, T. R.,  
862 Graham, I. M., & Lusseau, D. (2014). Scale-dependent foraging ecology of a marine  
863 top predator modelled using passive acoustic data. *Functional Ecology*, 28(1), 206-  
864 217. doi: 10.1111/1365-2435.12146  
865

866 Priede, I. G., & Miller, P. I. (2009). A basking shark (*Cetorhinus maximus*) tracked by  
867 satellite together with simultaneous remote sensing II: New analysis reveals  
868 orientation to a thermal front. *Fisheries Research (Amsterdam)*, 95(2-3), 370-372.  
869 doi: :10.1016/j.fishres.2008.09.038  
870

871 Queiroz, N., Humphries, N. E., Noble, L. R., Santos, A. M., & Sims, D. W. (2012). Spatial  
872 Dynamics and Expanded Vertical Niche of Blue Sharks in Oceanographic Fronts  
873 Reveal Habitat Targets for Conservation. *Plos One*, 7(2). doi:  
874 e3237410.1371/journal.pone.0032374  
875

876

877 Scales, K. L., Miller, P. I., Hawkes, L. A., Ingram, S. N., Sims, D. W., & Votier, S. C. (2014).  
878 On the Front Line: frontal zones as priority at-sea conservation areas for mobile

879 marine vertebrates. *Journal of Applied Ecology*, 51(6), 1575-1583. doi:  
880 10.1111/1365-2664.12330  
881  
882 Scales, K. L., Miller, P. I., Varo-Cruz, N., Hodgson, D. J., Hawkes, L. A., & Godley, B. J.  
883 (2015). Oceanic loggerhead turtles *Caretta caretta* associate with thermal fronts:  
884 evidence from the Canary Current Large Marine Ecosystem. *Marine Ecology*  
885 *Progress Series*, 519, 195-207. doi: 10.3354/meps11075  
886  
887  
888 Sharples, J. (2008). Potential impacts of the spring-neap tidal cycle on shelf-sea primary  
889 production. *Journal of Plankton Research*, 30(2), 183-197. doi:  
890 10.1093/plankt/fbm088  
891  
892 Shimada, T., Sakaida, F., Kawamura, H., & Okumura, T. (2005). Application of an edge  
893 detection method to satellite images for distinguishing sea surface temperature fronts  
894 near the Japanese coast. *Remote sensing of environment*, 98(1), 21-34.  
895  
896 Simpson, J. H., Crisp, D. J., & Hearn, C. (1981). The shelf-sea fronts: implications of their  
897 existence and behaviour [and discussion]. *Philosophical Transactions of the Royal*  
898 *Society of London A: Mathematical, Physical and Engineering Sciences*, 302: 531-546.  
899  
900 Simpson, J. H., Tett, P. B., Argote-Espinoza, M. L., Edwards, A., Jones, K. J. & Savidge.  
901 (1982). Mixing and phytoplankton growth around an island in a stratified sea.  
902 *Continental Shelf Research* 1(1): 15-31.  
903  
904 Simpson, J. H., & Sharples, J. (2012). *Introduction to the physical and biological*  
905 *oceanography of shelf-seas*: Cambridge University Press.  
906  
907 Stegmann, P. M., & Ullman, D. S. (2004). Variability in chlorophyll and sea surface  
908 temperature fronts in the Long Island Sound outflow region from satellite  
909 observations. *Journal of Geophysical Research: Oceans*, 109(C7).  
910  
911 Suberg, L. A. (2015). *Investigations of the variability of tidal mixing fronts and their*  
912 *importance for shelf-sea ecosystems across multiple trophic levels* (Unpublished  
913 doctoral thesis). University of Southampton, Faculty of Natural and Environmental  
914 Sciences, Southampton, UK.  
915  
916 Ullman, D. S., Cornillon, P. C., & Shan, Z. (2007). On the characteristics of subtropical fronts  
917 in the North Atlantic. *Journal of Geophysical Research-Oceans*, 112(C1). doi:  
918 C0101010.1029/2006jc003601  
919  
920 Wingfield, D. K., Peckham, S. H., Foley, D. G., Palacios, D. M., Lavaniegos, B. E., Durazo,  
921 R. & Bograd, S. J. (2011). The making of a productivity hotspot in the coastal ocean.  
922 *PloS one*, 6(11), e27874.  
923  
924 Wood, S. N. (2006). *Generalized Additive Models: An Introduction with R*. Chapman and  
925 *Hall/CRC*.  
926  
927 Xu, Y., Nieto, K., Teo, S. L., McClatchie, S., & Holmes, J. (2017). Influence of fronts on the  
928 spatial distribution of albacore tuna (*Thunnus alalunga*) in the Northeast Pacific over  
929 the past 30 years (1982–2011). *Progress in Oceanography*, 150, 72-78.  
930  
931 Young, E. F., Brown, J., Aldridge, J. N., Horsburgh, K. J., & Fernand, L. (2004).  
932 Development and application of a three-dimensional baroclinic model to the study of

933 the seasonal circulation in the Celtic Sea. *Continental Shelf Research*, 24(1), 13-36.  
934 doi: 10.1016/j.csr.2003.09.003  
935  
936  
937 Zuur, A. F., Ieno, E. N., Walker, N. J., Saveliev, A. A., Smith, G. M., & . (2009). *Mixed*  
938 *Effects Models and Extensions in Ecology with R*. New York.  
939  
940